

Collaborative Beamforming for Communication Applications Using a Two-Element Fully-Wireless Open-Loop Coherent Distributed Array

Jason M. Merlo, *Graduate Student Member, IEEE*, Jeffrey A. Nanzer, *Senior Member, IEEE*

Abstract—In this work we demonstrate a proof of concept of a fully-wireless two-node open-loop coherent distributed communication system and evaluate its performance by transmitting QPSK, 64-QAM, and 256-QAM constellations at a symbol rate of 2 MBd over a 58 m link in an urban environment. The system is implemented in a distributed manner with on-node processing using software-defined radios (SDRs) and wireless internode communication to share coordination information and does not rely on external time or frequency references such as the global navigation satellite system (GNSS). In each experiment ~ 100 messages were transmitted and a mean coherent gain of 0.936 was achieved across all measurements with a mean symbol error ratio of below 1.4×10^{-4} achieved up to 64-QAM, demonstrating a reliable bandwidth of up to 12 Mbps.

Index Terms—Communication systems, distributed antenna arrays, distributed beamforming, mobile communication, wireless communication, wireless sensor networks, wireless synchronization.

I. INTRODUCTION

Interest in wirelessly coordinated open-loop coherent distributed antenna arrays (CDAs) has been increasing in recent years due to their promise to enhance existing communication and sensing systems by providing increased scalability, increased reconfigurability, and increased robustness to element failure, with respect to traditional monolithic antenna arrays, since elements can be freely added, removed, and relocated at runtime to adapt to changing operational requirements [1]. Applications for CDAs include distributed sensing [2]–[4], microwave imaging [5], [6], wireless power transfer [7], [8], and terrestrial and space-based communication [9]–[11] [12, §TX05.2.6].

While the concept of CDAs has been around for decades [13], many experimental demonstrations have employed closed-loop beamforming using feedback from a designated receiver node [14], [15] which limits the application to cooperative communication scenarios; however, recent advances in wireless system coordination at the carrier wavelength [2], [16]–[19] have enabled experimental measurements of arrays using open-loop topologies where the

This effort was sponsored in whole or in part by the Central Intelligence Agency (CIA), through CIA Federal Labs. The U.S. Government is authorized to reproduce and distribute reprints for Governmental purposes notwithstanding any copyright notation thereon. The views and conclusions contained herein are those of the authors and should not be interpreted as necessarily representing the official policies or endorsements, either expressed or implied, of the Central Intelligence Agency.

J. M. Merlo and J. A. Nanzer are with the Department of Electrical and Computer Engineering, Michigan State University, East Lansing, MI 48824 USA (e-mail: merlojas@msu.edu; nanzer@msu.edu).

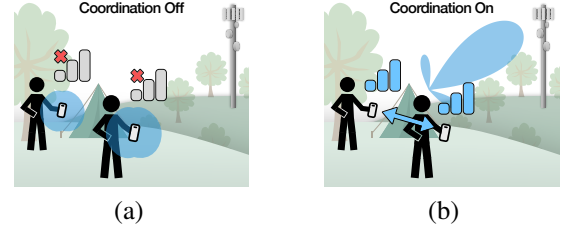


Fig. 1. Collaborative beamforming used in a communication scenario. In (a), an individual UE cannot access the base station (BS) due to a low signal gain. In (b), the UEs coordinate wirelessly to perform collaborative beamforming to increase signal gain and establish communication with the BS.

destination does not provide feedback to the transmit array. While there have been several notable experimental demonstrations of open-loop CDAs investigating their use in sensing and communication applications [2]–[4], [10], the majority of experimental demonstrations to this point have mainly focused sending continuous-wave (CW) tones to assess the array gain, but have not implemented applications running atop the array to identify and address challenges unique to CDAs, in practice.

The goal of this work is to demonstrate a two-node distributed communication system transmitter. A motivating example for this work is provided in Fig. 1, illustrating a CDA for use in a mobile communication application where two or more user devices (UEs) coordinate wirelessly to extend their range via collaborative beamforming. We build on the time and frequency coordination techniques described in [16] and [17] in a system similar to those described in [3], [17], but with performance improvements in two key areas: the system no longer requires a global navigation satellite system (GNSS) receiver for coarse time alignment; and the synchronization epoch duration has been reduced from ~ 100 ms to ~ 10 μ s, greatly improving the resiliency to dynamic environmental multipath. In these experiments, we use quadrature amplitude modulation (QAM) constellations, first with a low order quadrature phase-shift keying (QPSK), then with 64-QAM and 256-QAM constellations. The added gain of the array from the second node is evaluated using a series of CW pulses in the preamble, the carrier phase alignment is evaluated through orthogonal Zadoff–Chu (ZC) sequences transmitted in the preamble, and the error vector magnitude (EVM) and symbol error ratio (SER) are evaluated based on the transmission of pseudo-random sequences in the QAM payload waveforms.

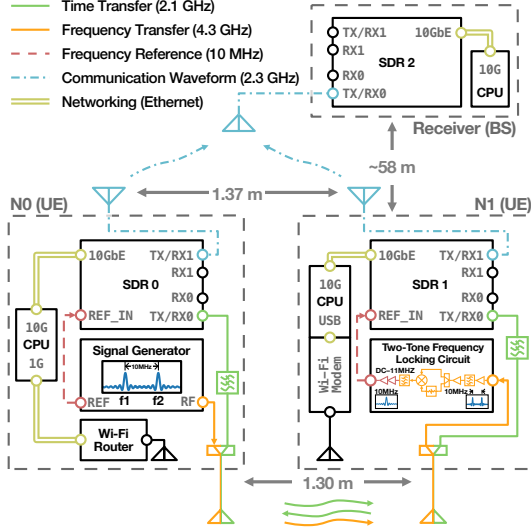


Fig. 2. Distributed transmit system schematic. The system used two transmitting nodes which were wirelessly coordinated time and frequency to beamform communication waveforms. An unsynchronized receive node was located 58 m down-range and recorded data for demodulation.

II. DISTRIBUTED TRANSMIT BEAMFORMING COMMUNICATION SYSTEM

The primary challenge with wirelessly coordinated distributed systems is ensuring that they sum coherently at the receiver. To accomplish this, the time, frequency, and phase offsets between each system must be estimated and compensated for down to a fraction of a carrier wavelength [1]. To model this, we represent the transformation between the global true time t and the local time at any node n as

$$T^{(n)}(t) = \alpha^{(n)}(t)t + \delta^{(n)}(t) + \nu^{(n)}(t) \quad (1)$$

where $\alpha^{(n)}(t)$ is the time-varying relative frequency scaling coefficient, $\delta^{(n)}(t)$ is the time-varying time bias, and $\nu^{(n)}(t)$ is a zero-mean noise term due to device properties such as thermal noise, flicker noise, shot noise, etc. It should be noted that, in general the transmit and receive pathways of a radio will have separate functions T to represent their offset due to having unique time and phase delays in their respective radio frequency (RF) pathways. The RF carrier can be modeled by

$$\Phi_{\text{RF}}^{(n)}(t) = \exp\left\{j \left[2.0\pi f_{\text{RF}} T^{(n)}(t) + \phi_0^{(n)} \right] \right\} \quad (2)$$

where f_{RF} is the intended carrier frequency and ϕ_0 is the initial phase of the local oscillator (LO).

To ensure the transmitted waveforms sum coherently at the receiver, the transmitters need to estimate and compensate for: relative frequency offset between systems $\alpha^{(n)}$, relative time offset between systems $\delta^{(n)}$, and the inter-arrival phases of the waveforms transmitted from each node. Assuming the systems are synchronized—aligned in frequency—the inter-arrival phases are a function of the initial LO phase $\phi_0^{(n)}$, the phase delay induced by $\delta^{(n)}$, and the relative locations of the transmitting and receiving nodes. In this work we establish the initial phase offset of each RF front-end and relative node locations by performing an initial far-field calibration to the receiving node. Thus, only $\delta^{(n)}$ must be continuously estimated online.



Fig. 3. Photograph of the distributed transmit array (foreground) and receive node (inset). Node 0 is located on the left, and Node 1 is located on the right. Log-periodic antennas on wooden masts were used for time-frequency coordination as well as beamforming and can be seen on top of the carts.

To align the LO frequencies between systems and compensate for $\alpha^{(n)}$, a two-tone CW reference tone was transmitted from UE node 0 (the primary node) and demodulated using self-mixing circuit described in [9], [16]; this provides a fixed relative phase between nodes in static environments. To align the time and phase, we use the technique described in [17], which uses a two-way time transfer process with a quadratic least-squares refinement process and lookup table-based bias compensation phase. To compensate for the time and calibrated phase, a delay and phase is applied to the sampled baseband waveform. The baseband compensation waveform to be added at each node is

$$s_{\text{comp}}^{(n)}(t) = \exp \left\{ -j \left[2.0\pi f_{\text{RF}} \tilde{\delta}^{(n)}(t) + \tilde{\phi}_0 \right] \right\} \quad (3)$$

where $\tilde{(\cdot)}$ represents an estimated quantity. Thus, the total waveform transmitted from each node after applying compensation and baseband modulation can be modeled as

$$s^{(n)}(t) = \Phi_{\text{RF}}^{(n)}(t) s_{\text{comp}}^{(n)}(t) s_m(T^{(n)}(t)) \quad (4)$$

where $s_m(t)$ is the desired baseband message to be transmitted—in this case a QAM message.

III. EXPERIMENTAL CONFIGURATION AND RESULTS

The experimental system is shown schematically in Fig. 2 and photographed in Fig. 3. Each UE node was separated by ~ 1.3 m and contained an Ettus Research X310 software-defined radio (SDR) connected to a Dell Optiplex 7080 desktop. Each node communicated over TCP/IP using ZeroMQ via Wi-Fi.

The time and frequency coordination waveforms were transmitted between nodes using shared log-periodic antennas. The primary node N0 contained a signal generator which acts as the primary LO for the system; the 10 MHz output was used to directly discipline the LO on SDR 0 while a two-tone CW waveform was transmitted at 4305 MHz as reference for UE N1. N1 demodulated the frequency reference using the two-tone frequency locking circuit and use the 10 MHz output to discipline the LO on SDR 1. The time transfer operation was performed using channel 0 on each SDR at 2100 MHz. The initial fine time-phase acquisition process utilized TCP/IP packets transmitted between nodes to query the local times on each radio which provided an initial estimate on the order of 10 ms; after initial network-based time alignment, the nodes would send a pulsed two-tone waveform synchronization waveform with a low tone separation (1 MHz) at a low sample

Trigger ZC (29)	Coherent Gain CW (28)	Node ID ZC (29)	Start of Data ZC (29)	Data {4,64,256}-QAM (1024)
--------------------	-----------------------------	--------------------	-----------------------------	----------------------------------

Fig. 4. Message structure. Preamble contained four sequences, three of which were 29-symbol Zadoff-Chu (ZC) sequences, and the fourth was a set of continuous-wave (CW) pulses intended to evaluate carrier phase coherence of the system. Three data modulation schemes were evaluated: QPSK, 64-QAM, and 256-QAM.

rate (10 MSa/s) with a wide time-domain multiplexing (TDM) window duration, then iteratively increase the sample rate and tone separation while reducing the TDM window to values of 20 MHz, 200 MSa/s, and 10 μ s; in all cases, pulse durations of 2 μ s were used.

The beamforming waveform was transmitted from each node using an 8-dBi log-periodic antenna at 2300 MHz at a sample rate of 200 MSa/s with a symbol rate of 2 MBd. A root-raised-cosine window was applied to each symbol with a duration of 41 symbols and a roll-off factor of 0.3. The message used a four-part preamble consisting of a trigger, coherent gain estimation pattern, node identifier, and start of data indicator, shown in Fig. 4. The trigger, node identifier, and start of data indicator were all 29-symbol ZC sequences where the node identifiers were unique for each UE. The coherent gain estimation waveform consisted of 4-symbol long constant-phase pulses where first UE N0 would transmit, then UE N1 would transmit, then both UEs would transmit simultaneously so that the total coherent gain G_c could be estimated, where G_c is the fraction of the measured combined pulse's amplitude relative to the ideal summation of each of the individual pulse amplitudes. The node identifier was used for calibration and performance evaluation since the individual nodes magnitude and phase could be estimated by matching filtering to the orthogonal ZC sequence. The payload of the message contained 1024 symbols of pseudo-random QAM data using QPSK, 64-, and 256-QAM schemes. The receiver base station (BS) node was placed 58 m downrange and used a similar desktop computer and SDR configuration as the transmitters, but because it was not time synchronized with the transmitter UEs, it was run in a continuous streaming mode which limited the receive sample rate to 50 MSa/s. A matched filter for the trigger preamble was run on the data in real-time to save the waveforms for offline evaluation and demodulation.

The data collection process for each constellation type consisted of both an uncalibrated control measurement where front-end calibrations were not applied (but time and frequency coordination was still operational) and a calibrated measurement where the front-end was calibrated ahead of time to the receiver location using the node identifier preamble to estimate inter-node time and phase of arrival corrections; after the calibration process the program was restarted and the calibrated measurements were taken. For each modulation order 100–110 messages were collected and used to compute the inter-node carrier phase offsets, coherent gain, EVM, and SER at the receiver. A summary of these statistics is shown in Fig. 5. The relative inter-arrival phase is shown in the first row and illustrates the impact of proper phase alignment between

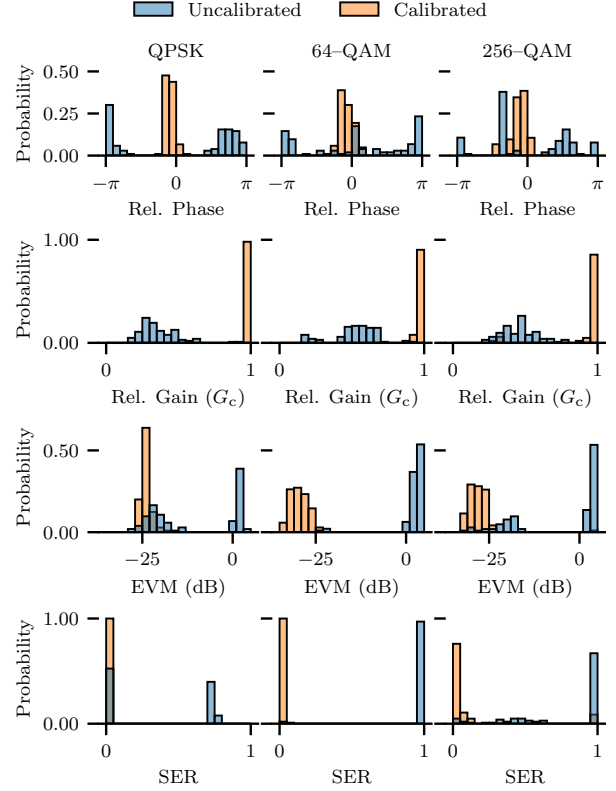


Fig. 5. Measured performance metrics for QPSK, 64-, and 256-QAM. Top to bottom are relative inter-arrival phase, coherent gain relative to ideal summation, error vector magnitude (EVM), symbol error ratio (SER).

the nodes; in the calibrated case, the phase due to static differences in the RF front-end, transmission lines, antenna patterns, and propagation distances are corrected. The second row illustrates the improvement in coherent gain performance after calibration which resulted in a mean coherent gain improvement from 0.442 for the uncalibrated case to 0.963 after calibration. The third and fourth rows shown the EVM and SER, respectively, and illustrate the data demodulation performance improvement after calibration. In both the QPSK and 64-QAM cases, the SER was below 1.4×10^{-4} , while the SER of the 256-QAM modulation was higher, possibly due to slight signal compression, and several unrecoverable messages due to carrier frequency offset estimation failure which was not observed in other modulation orders, which may have been caused by out of band interference.

IV. CONCLUSION

In this work, we demonstrate initial measurements of a CDA transmitter for collaborative communication beamforming applications in an urban environment. We show excellent performance for QPSK and 64-QAM constellations and promising results for higher order modulation schemes with further tuning. A coherent gain of 0.936 was achieved across all measured waveforms, and a SER of below 1.4×10^{-4} was obtained up to 64-QAM enabling raw bitrates of up to 12 Mbps. These results show encouraging performance and motivate further work studying scaling array sizes and symbol rates for future efforts.

REFERENCES

- [1] J. A. Nanzer, S. R. Mghabghab, S. M. Ellison, and A. Schlegel, "Distributed phased arrays: Challenges and recent advances," *IEEE Transactions on Microwave Theory and Techniques*, vol. 69, no. 11, pp. 4893–4907, 2021.
- [2] S. Prager, M. S. Haynes, and M. Moghaddam, "Wireless subnanosecond rf synchronization for distributed ultrawideband software-defined radar networks," *IEEE Transactions on Microwave Theory and Techniques*, vol. 68, no. 11, pp. 4787–4804, 2020.
- [3] J. M. Merlo, S. Wagner, J. Lancaster, and J. A. Nanzer, "Fully wireless coherent distributed phased array system for networked radar applications," *IEEE Microwave and Wireless Technology Letters*, vol. 34, no. 6, pp. 837–840, 2024.
- [4] D. Werbunat, B. Woischneck, J. Lerch, B. Schweizer, R. Michev, C. Bonfert, J. Hasch, and C. Waldschmidt, "Multichannel repeater for coherent radar networks enabling high-resolution radar imaging," *IEEE Transactions on Microwave Theory and Techniques*, vol. 72, no. 5, pp. 3247–3259, 2024.
- [5] D. Luzano, J. M. Merlo, D. Chen, J. R. Colon-Berrios, A. Bhattacharyya, and J. A. Nanzer, "A distributed microwave correlation interferometer for fourier domain imaging using wireless time and frequency coordination," in *2024 IEEE International Symposium on Antennas and Propagation and INC/USNC-URSI Radio Science Meeting*, 2024, pp. 1455–1456.
- [6] T. Nusrat and S. Vakalis, "Addressing specularly: Millimeter-wave radar with distributed repeater apertures," *IEEE Transactions on Microwave Theory and Techniques*, pp. 1–10, 2024.
- [7] J. Brunet, A. Ayling, and A. Hajimiri, "Transmitarrays for wireless power transfer on earth and in space," *IEEE Journal of Microwaves*, pp. 1–12, 2024.
- [8] K. W. Choi, A. A. Aziz, D. Setiawan, N. M. Tran, L. Ginting, and D. I. Kim, "Distributed wireless power transfer system for internet of things devices," *IEEE Internet of Things Journal*, vol. 5, no. 4, pp. 2657–2671, 2018.
- [9] O. Abari, H. Rahul, D. Katabi, and M. Pant, "Airshare: Distributed coherent transmission made seamless," in *2015 IEEE Conference on Computer Communications (INFOCOM)*, 2015, pp. 1742–1750.
- [10] J. Holtom, O. Ma, A. Herschfelt, I. Lenz, Y. Li, and D. W. Bliss, "Distributed coherent mesh beamforming (discobeam) for robust wireless communications," *IEEE Transactions on Wireless Communications*, vol. 23, no. 11, pp. 15 814–15 828, 2024.
- [11] M. B. Quadrelli, R. Hodges, V. Vilnrotter, S. Bandyopadhyay, F. Tassi, and S. Bevilacqua, "Distributed swarm antenna arrays for deep space applications," in *2019 IEEE Aerospace Conference*, 2019, pp. 1–15.
- [12] "2020 NASA technology taxonomy," National Aeronautics and Space Administration, Tech. Rep. HQ-E-DAA-TN76545, Jan. 2020.
- [13] H. Ochiai, P. Mitran, H. Poor, and V. Tarokh, "Collaborative beamforming for distributed wireless ad hoc sensor networks," *IEEE Transactions on Signal Processing*, vol. 53, no. 11, pp. 4110–4124, 2005.
- [14] P. Bidigare, M. Oyarzyn, D. Raeman, D. Chang, D. Cousins, R. O'Donnell, C. Obranovich, and D. R. Brown, "Implementation and demonstration of receiver-coordinated distributed transmit beamforming across an ad-hoc radio network," in *2012 Conference Record of the Forty Sixth Asilomar Conference on Signals, Systems and Computers (ASILOMAR)*, 2012, pp. 222–226.
- [15] F. Quitin, M. M. U. Rahman, R. Mudumbai, and U. Madhow, "A scalable architecture for distributed transmit beamforming with commodity radios: Design and proof of concept," *IEEE Transactions on Wireless Communications*, vol. 12, no. 3, pp. 1418–1428, 2013.
- [16] S. R. Mghabghab and J. A. Nanzer, "Open-loop distributed beamforming using wireless frequency synchronization," *IEEE Transactions on Microwave Theory and Techniques*, vol. 69, no. 1, pp. 896–905, 2021.
- [17] J. M. Merlo, S. R. Mghabghab, and J. A. Nanzer, "Wireless picosecond time synchronization for distributed antenna arrays," *IEEE Transactions on Microwave Theory and Techniques*, vol. 71, no. 4, pp. 1720–1731, Dec. 2022.
- [18] R. H. Kenney, J. G. Metcalf, and J. W. McDaniel, "Wireless distributed frequency and phase synchronization for mobile platforms in cooperative digital radar networks," *IEEE Transactions on Radar Systems*, vol. 2, pp. 268–287, 2024.
- [19] J. Aguilar, D. Werbunat, V. Janoudi, C. Bonfert, and C. Waldschmidt, "Uncoupled digital radars creating a coherent sensor network," *IEEE Journal of Microwaves*, vol. 4, no. 3, pp. 459–472, 2024.